A Displacement Uncertainty Model for 2-D DIC Measurement Under Motion Blur Conditions

Alberto Lavatelli, *Member, IEEE*, and Emanuele Zappa, *Member, IEEE*

Abstract—In this paper, the effects of motion blur on 2-D digital image correlation (DIC) measurements are discussed, with a particular focus on the description of displacement measurement uncertainty. The research started with the simulation of motion blur with a suitable literature-based algorithm. Then the state of the art of uncertainty analysis in the context of DIC was compared with simulation results, and it was found that the effects of motion blur on uncertainty are not predicted correctly by the literature models. This phenomenon is explained by the fact that the literature models do not consider motion blur. Consequently, a simple monodimensional case is analyzed. In this way, it has been possible to evaluate the sensitivity of DIC correlation function [evaluated as the sum of squared differences (SSD)] to motion blur. Using these results, it is possible to extend the analysis to the case of a generic image with the help of a power-law model. Eventually, the model proposed in this paper is able to represent the effects of motion blur correctly.

Index Terms—2-D DIC, analytic model, digital image correlation (DIC), displacement uncertainty, motion blur, uncertainty analysis.

I. Introduction

THE goal of this paper is to investigate the effects of motion blur on displacement measurement uncertainty in the field of 2-D digital image correlation (DIC) techniques. DIC uncertainty is composed of two contributes [1]: a correlation bias (namely bias error) [2], [3] and a random error [4], for which the measured displacement is characterized by dispersion even when a uniform displacement field is imposed. For what concerns the object of interest of this paper, it has been demonstrated [5], [6] that random error is the main uncertainty component in the presence of motion blur. The bias error, although existing and relevant in the subpixel region [7], [8] is almost negligible in the presence of motion blur. Hence, our aim is to model the process that defines how the standard deviation of measured displacement is influenced by motion blur. In spite of numerous applications of DIC in dynamic contexts, only little is known about how the descriptive parameters of a generic pattern (in-center spacing, mean image gradient, speckle size, or variability) influence the sensitivity to motion blur.

In other words, the aim of this paper is to analyze how motion blur deteriorates the acquired patterns and how this deterioration interferes with measurement uncertainty. After having reviewed the most recent literature, the effects of motion blur in terms of image degradation and measurement uncertainty are derived exploiting a monodimensional analysis framework. The analysis of monodimensional framework is then extended to real patterns with the help of a power law model hypothesis. This assumption is done on the basis of the monodimensional analysis previously proposed and then verified with the help of a synthetic experiment, where displacement and motion blur are generated with appropriate methods. In conclusion, the model developed in this paper is claimed to be of practical use in the prediction of the uncertainty contribute of motion blur as a function of the characteristics of the pattern and to understand the role of DIC pattern design into the rejection of errors due to motion blur.

II. Related Works

Digital image correlation is a broadly applied measurement technique in the field of experimental mechanics. The growth and diffusion of the aforementioned methodology is due to the relative ease to measure full field displacement and strain for both large-surface/large-scale deformation [9] and microstructure/nanoscale deformation [10], and, in general, DIC measurements are a valuable tool to solve complex problems in modeling the mechanical behavior of materials [11].

Starting from the early days [12], the diffusion of DIC application pushed the scientific community to investigate uncertainty for DIC measurements since the level of confidence in an experimental result is of key importance for decision makers. However, the qualification of uncertainty in this context required a dedicated research field to be developed within the scientific community in order to deal with high complexity of the DIC problem. On one side, understanding the errors of the image formation is complicated in itself, and on the other side, the correlation algorithm provides measurements after a complex cascade of image processing operations. The flow of information and possible error sources in DIC begins with the experimental setup, which includes the camera, lens, all the mounting hardware, and the whole recorded scene (Table I). While it is convenient and rather common to ignore all of these error inputs to the image, they may become critical. The common assumption that the image is a perfect reflection of the underlying measurand is incorrect, with many researchers mainly focusing on the image correlation step.

TABLE I

SOURCES OF UNCERTAINTY QUANTIFIABLE BY PRESENT LITERATURE

Experimental setup	Image formation	Image correlation	Displacement analysis
Camera Motion	Noise	Interpolant	Filtering
Sample motion	Contrast	Minimization	Strain calc.
Air turbulence	Speckle size	Shape function	Coord. system
Defocusing	Aliasing	Subset size	
Resolution			
Lighting			
Thermal radiation			

Algorithm 1 Exact Phase Shift and Averaging Algorithm

1: $I(i, j)$ {Load original image}
2: $S(i, j)$ {Calculate image spectrum (2D FT)}
3: X {Select a motion vector}
4: $Im(i, j, k)$ {Create an image array}
5: $p = 0 : \frac{X}{100} : X$ {Create a motion vector}
6: **for** $k = 1 : \texttt{length}(p)$ **do**
7:     phase shift original image spectrum
    $R(i, j) = S(i, j) \cdot e^{2\pi j \cdot [p(k,1)f_i + p(k,2)f_j]}$
8:     get rigid translation image
    $Im(:, :, k) = \texttt{ifft}(R(i, j))$
9:     add random Gaussian noise
    $Im(:, :, k) = Im(:, :, k) + \texttt{noise}$
10: **end for**
11: $B = \texttt{zeros}(i, j)$ {Create empty motion blurred image}
12: **for** $k = 1 : \texttt{length}(p)$ **do**
13:     $B(:, :) = B(:, :) + Im(:, :, k)$
14: **end for**
15: $B(:, :) = B(:, :)/\texttt{length}(p)$ {Calculate the motion blurred image as the average of all rigid translated frames}

However, in the last decade, the scientific community devoted big effort in analyzing and evaluating DIC measurement errors. The work of Schreier *et al.* [3] and Bornert *et al.* [1] defined clearly how to assess DIC measurement errors and how to evaluate their effect in the computation of the mechanical quantities. The interaction between DIC and optical phenomena has been broadly analyzed, with [13] defining the relationship between camera sampling efficiency and DIC accuracy. In [14] and [15], the effects of lens distortion on strain calculation have been analyzed. In [16], a methodology to assess pattern quality is formalized, while in [17], the theory of optimal design of patterns for static strain measurement is discussed. More recently, the interaction between radiation and image correlation was studied, with [18] providing models to describe systematic errors due to camera heating and [19] proposing a way to reduce the effects of the noise coming thermal radiation on DIC measurements. Lately, the problem of pattern degradation due to high strain is approached with experimental [20] and theoretical analysis [21]. All the previous listed efforts provided the experimenter with a set of useful tools to predict the contribute to uncertainty given by the phenomena listed in Table I, so that, today, it is possible to provide reasonable error budgets for the general application in a static condition [6], [22], [23]. Even if it is possible to model most of the common sources of uncertainty, as for today, the scientific community is missing a widely accepted tool able to quantify the contribution of motion blur to the total amount of uncertainty on a reliable and repeatable basis. This situation represents a weak point of many of the tracked application of DIC in the context of dynamic strain/displacement measurement. In the early documented dynamic applications of DIC [24], [25], the problem of motion blur was already seen as a relevant one; however, the experimenter chose to avoid the quantification of this component by limiting exposure time at a lowest-as-possible value. This result is achieved by boosting lighting at really high levels with the help of pulsed light. Even recent applications of DIC in the context of dynamic measurements see the experimenter dealing with the motion blur in the same way described before [26], [27].

Despite the general lack in the quantification of motion blur effects, the application of DIC in the context of very large structure pushes the investigation in this sense. The most recent experiences have been reviewed in [28], where the application of DIC as a measurement source for modal analysis is well documented. It is possible to find several successful case studies. The first experiences started with the extraction of mode shapes with monomodal excitation [29]–[31]. More recently, Poozesh *et al.* [32], [33] successfully extracted operating mode shapes of large-scale structures and the latest works sees the application of DIC for nonlinear dynamics experimental studies [34]. In most of the reviewed works, the experimenters highlighted relevant differences between the uncertainty predicted by means of static calibration-based analysis and the effective one. In order to answer to these questions, part of the scientific community developed several works in order to deal with motion blur uncertainty contribute: some have studied the effect of motion blur from a phenomenological point of view [5], [35], others proposed experimental benchmark in order to qualify uncertainty [6], [36], yet others proposed to merge the classic DIC analysis of uncertainty with the ones used in other fields of image processing [37], and the latest analysis propose also theoretical frameworks [38], [39].

III. NUMERICAL SIMULATION OF MOTION BLUR

In order to investigate uncertainty, a numerical experiment has been run. Four different DIC patterns have been selected (Fig. 1). The first two patterns have been selected among the ones publicly available at the SEM DIC challenge Web site [40]. Pattern #1 is selected as a "worst case" since it has a poor edge definition and its contrast is low. Pattern #2, conversely, is sharper and with higher contrast. Pattern #3 is an image of pattern #4 acquired by a digital camera. Pattern #4 is a numerically generated one, which is treated with a plain Gaussian blur mask of 4×4 pixels.

Each pattern has been submitted to a motion blur-translation transformation using Algorithm 1 [35], [41].

The motion blurred image output $B(i, j)$ represents the original image $I(i, j)$ rigidly translated by $(X/2)$ pixels and motion blurred by $W = X$ pixels. As a consequence, the
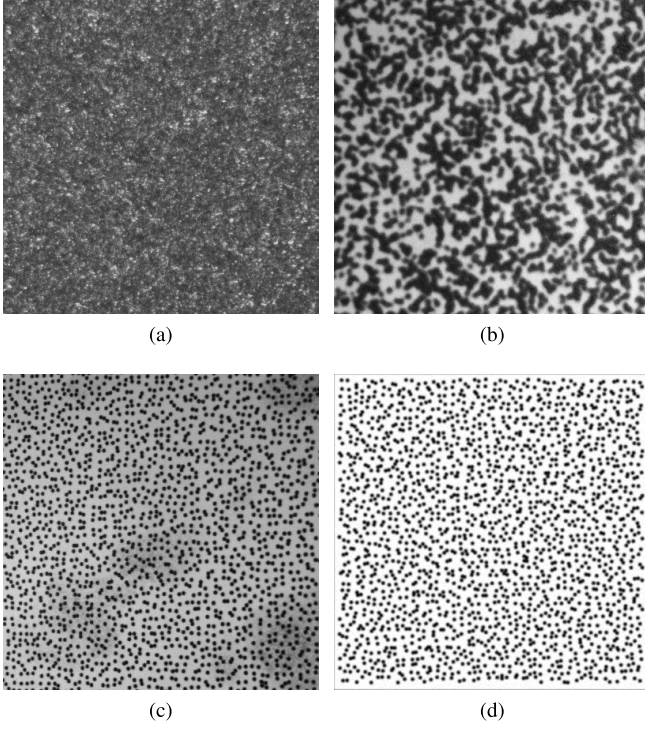
Fig. 1. Different patterns used for model testing. (a) #1 - SEM DIC Chall. Samp. 13. (b) #2 - SEM DIC Chall. Samp. 3. (c) #3 - Experimental. (d) #4 - Numerical pattern.

Fig. 2. Comparison among the Pan model and the motion blur simulation data. The maximum amount of motion blur W tested here is 11 px.

amount of motion blur W is defined as the length traveled by the image features during exposure time. Of course, it is possible to generate images with rigid motion different from $X/2$ by simply adding a constant to the values of p (step 5 of the algorithm). However, it was verified [35] that the value of rigid motion does not affect the uncertainty due to motion blur: even if in static conditions, the error depends mainly on fractional displacements [8]; in dynamic conditions, the random fluctuations due to motion blur are considerably higher in magnitude than the pixel locking phenomenon. Therefore, the results further displayed are computed without loss of generality.

Motion blur is investigated in the 0.1–10 px range, with 0.1 px step. The path covers the range of practical use of imaging devices in measurement activities up to the high motion blur range. Motion blur higher than 2 px is usually avoided in practical laboratory applications; however, when working with natural light and high-resolution imaging in field applications [32], [42], it is common to experiment high values of motion blur, especially when the measurand reaches velocity peaks.

IV. CORRELATION MATCH SCORE UNCERTAINTY MODEL FOR STATIC CONDITIONS

As stated previously, the analysis will focus on the random error due to motion blur, whose behavior is mainly driven by the SSSIG quantity (sum of square of subset intensity gradient) of (1) where $f(x, y)$ is the pixel intensity at a point (x, y) in the original image, N is the subset size, n is the number of
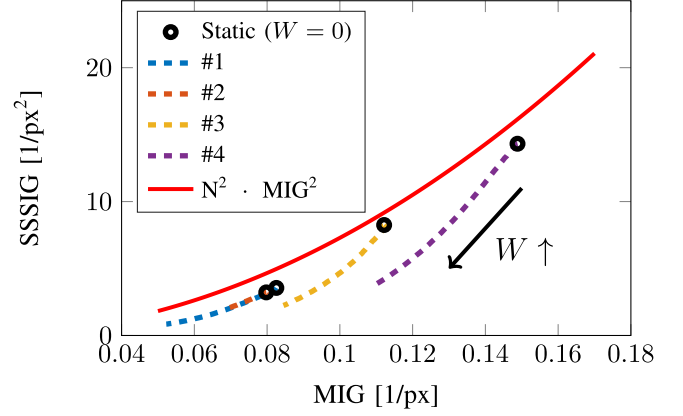
pixels in the x direction, and $x_{i,j}$ the single pixel

$$\text{SSSIG} = \sum_{i,j=1}^{N} \left(\frac{\partial f}{\partial x} \bigg|_{x_{ij}} \right)^2. \tag{1}$$

Considering a situation where DIC measurement is performed on a rigidly translated target, the SSSIG is helpful to quantify the standard deviation u_e of subset displacement (which should be null in the ideal case). As shown in [43], u_e can be evaluated with (2)

$$u_e = \sqrt{\frac{2 \cdot \sigma_N^2}{\text{SSSIG}}} \tag{2}$$

where σ_N represents the standard deviation of image noise. This model is known in the literature as the match score model. Its formulation is not universal, since it does not consider the effect of fractional part of displacement (relevant in static conditions [44], [45]), but it manages the random component. This model has spread widely due to its ability to quantify the random error (and its rejection) from the characteristics of a DIC pattern. In order to improve the practical application of 2, Pan *et al.* [46] then introduced an approximation of the SSSIG quantity as follows:

$$\text{SSSIG} \approx N^2 \cdot \text{MIG}^2 \tag{3}$$

where MIG stands for mean image gradient and it is calculated as the average value of the modulus of omnidirectional image gradient within the DIC pattern

$$MIG = \frac{1}{m \cdot n} \sum_{i,j=1}^{m,n} \left[\sqrt{\left(\frac{\partial f}{\partial x} \bigg|_{x_{ij}} \right)^2 + \left(\frac{\partial f}{\partial y} \bigg|_{x_{ij}} \right)^2} \right]. \tag{4}$$

By substitution the final expression of u_e proposed by Pan becomes

$$u_e \approx \frac{\sqrt{2} \cdot \sigma_N}{N \cdot MIG}. \tag{5}$$

Fig. 2 shows the trend of SSSIG approximated with the model proposed by Pan (3) and the results of the numerical analysis proposed in this paper. Pan's model deals with static conditions (no motion blur); therefore, it should be compared with the

static points in Fig. 2. The model proposed by Pan introduces an approximation, since the inequality displayed in (6) is valid for the general pattern. The discrepancy between the two terms of (6) can be very low for some types of patterns, while somewhat larger for others. This explains why it is possible to see different discrepancies between the static point and the Pan approximation represented by the red line in Fig. 2. For what concerns the patterns of Fig. 1, it is possible to see in Fig. 2 that the static point of pattern #3 lies close to the Pan approximation. Oppositely, the other patterns are less close to the hypothesis formulated by Pan

$$\sqrt{\sum_{i,j=1}^{N}\left(\left.\frac{\partial f}{\partial x}\right|_{x_{ij}}\right)^2} \neq \sum_{i,j=1}^{N}\sqrt{\left(\left.\frac{\partial f}{\partial x}\right|_{x_{ij}}\right)^2}. \quad (6)$$

In any case, the models of (2) and (5) were developed in the case of static measurement, so that image noise plays the main role, and for those particular patterns that verify (3). To be more precise, the pattern formulation that can be addressed with the Pan formula should respect the constraints of (7)

$$\begin{cases} \int \left(\frac{\partial f}{\partial x}\right)^2 dx - \left(\int \left|\frac{\partial f}{\partial x}\right| dx\right)^2 = 0 \\ \int \left(\frac{\partial f}{\partial y}\right)^2 dy - \left(\int \left|\frac{\partial f}{\partial y}\right| dy\right)^2 = 0. \end{cases} \quad (7)$$

Coming to the numerical experiment object of this paper, the values of $SSSIG$ and MIG decrease as motion blur increases (Fig. 2). Differently to what happens for the static case, the value of $SSSIG$ of the image with motion blur may be sensibly different from the reference image. This phenomenon quantifies the degradation of the image due to motion blur. Considering that the correlation match score expressed in (2) addresses the situation where the reference pattern and the acquired one have similar value of $SSSIG$, it is not possible to use it to estimate and model uncertainty arising from motion blur. Hence, it is necessary to develop a dedicated tool starting from the analysis of a simple case.

V. ANALYSIS OF MOTION BLUR EFFECTS ON A PERIODIC PULSE SIGNAL

In order to model the contribution of motion blur to DIC uncertainty, let us consider a monodimensional signal $p(x)$, consisting of a periodic repetition of rectangular pulses of height a, width d_p, in-center spaced by d_u pixels, as shown in Fig. 3. This type of simplified analysis is a simple case for sure, but it allows the development of a meaningful sensitivity analysis, since the three aforementioned parameters play a major role in the description of uncertainty for DIC measurements as documented in the literature [47]–[50].

The motion blur is then modeled as a signal convolution process with a rectangular uniform convolution window of width $\tilde{w}$. In other words, the signal resulting from convolution is the moving average over $\tilde{w}$ pixels of the original signal. It is important to define with (8) what is the relationship between the width of motion blur W as defined in Section III and the quantity $\tilde{w}$

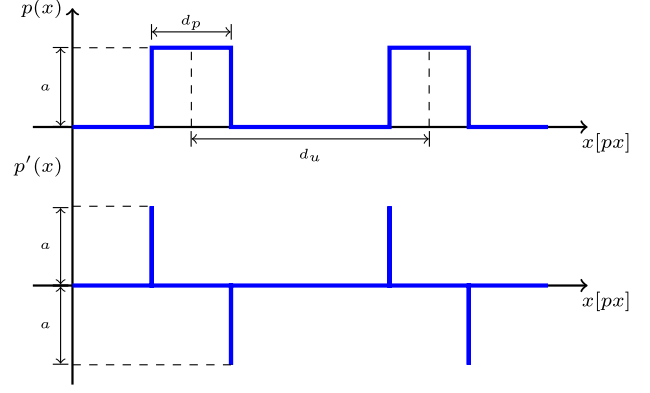$$\tilde{w} = 1 + W. \quad (8)$$

Fig. 3.   Monodimensional grid used by the model.

Consequently, the values of window width $\tilde{w}$ span from 1 (i.e., no motion blur) to $+\infty$. Considering the simple nature of a monodimensional scheme, it is possible to predict the effects of motion blur by mathematical analysis, resulting in the signals of Fig. 4. Once the signals are retrieved, it is necessary to express the value of the quantities of interest for the analysis of uncertainty in (9)

$$\begin{cases} MIG = \frac{1}{N}\sum_{i=1}^{N}\left[\sqrt{\left(\left.\frac{\partial f}{\partial x}\right|_{x_i}\right)^2}\right] \\ \text{var}[p'(x)] = \frac{1}{N}\sum_{i=1}^{N}\left[\left(\left.\frac{\partial f}{\partial x}\right|_{x_i} - \left\langle\left.\frac{\partial f}{\partial x}\right|_{x_i}\right\rangle\right)^2\right] \\ SSSIG = \sum_{i=1}^{N}\left(\left.\frac{\partial f}{\partial x}\right|_{x_i}\right)^2. \end{cases} \quad (9)$$

In particular, it is important to highlight that, given the pulse shape, the average value of image gradient $p'(x)$ is identically equal to 0. It is interesting to see that even in the case of a real DIC pattern, it is possible to assume that the average value of image gradient is about 0. This last condition means having a uniform mean brightness value over the image. Consequently, it is possible to write

$$\begin{cases} \left\langle\left.\frac{\partial f}{\partial x}\right|_{x_i}\right\rangle = 0 \\ \text{var}[p'(x)] = \frac{1}{N}\sum_{i=1}^{N}\left[\left(\left.\frac{\partial f}{\partial x}\right|_{x_i}\right)^2\right] \\ \text{rms}[p'(x)] = \sqrt{\text{var}[p'(x)]}. \end{cases} \quad (10)$$

It is now possible to express the value of $SSSIG$. It is necessary to specify what is intended for subset; in this case, without loss of generality, the subset size N represents the number of pulses included in a single subset. As a consequence, for each case of motion blur size, the $SSSIG$ value is expressed by the following:

$$SSSIG = N \cdot \text{var}[p'(x)]. \quad (11)$$

Given all the previous premises, it is now possible to analytically calculate the motion blurred signal as well as the values of the quantities expressed in (9). The results are shown in Fig. 4 and Table II, respectively.
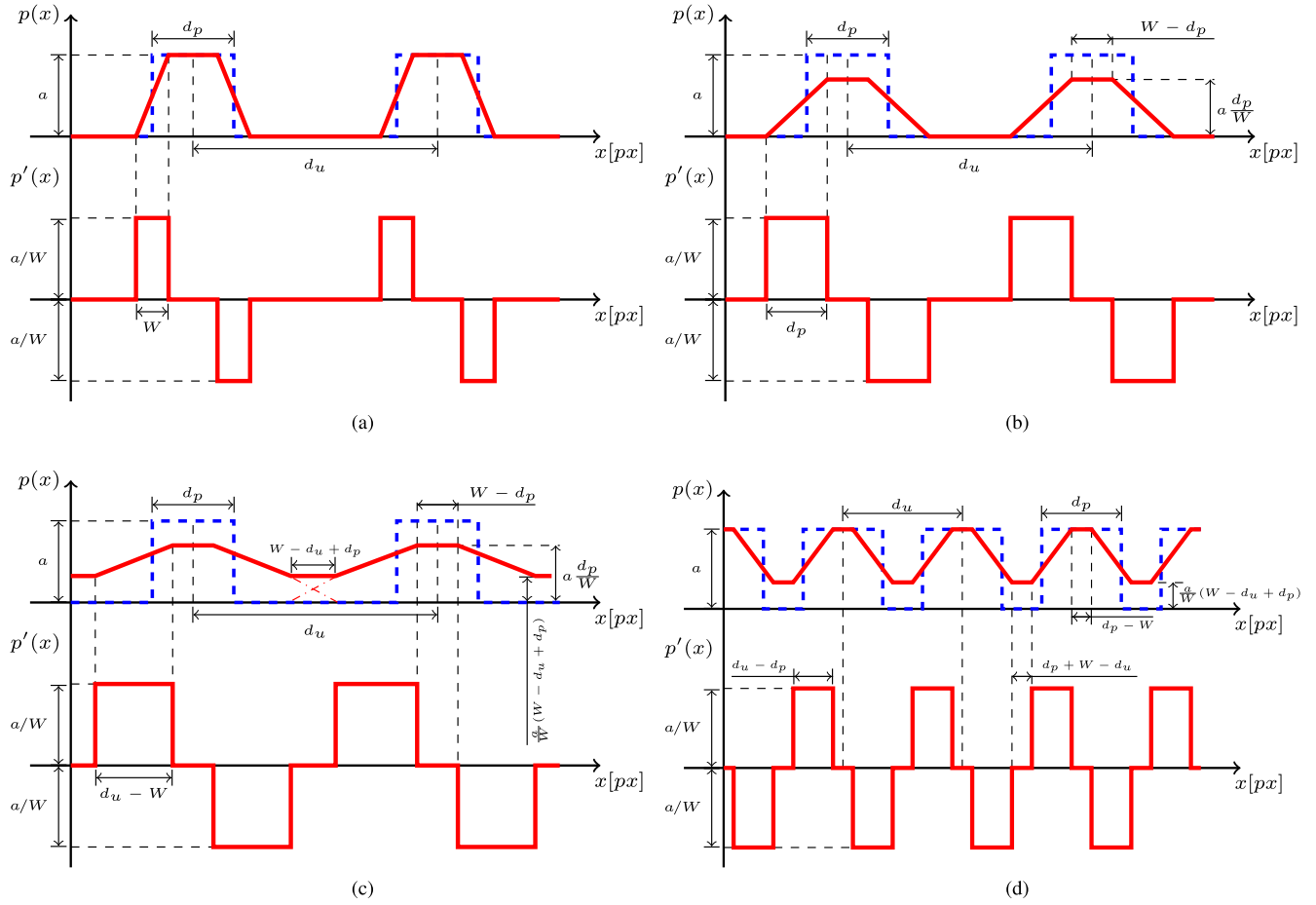
Fig. 4. Different cases of convolution effects on a periodic pulse signal. Blue dashed line: original signal. Solid red line: convoluted signal. (a) $\tilde{w} < d_p$; $\tilde{w} < d_u - d_p$. (b) $\tilde{w} > d_p$; $\tilde{w} < d_u - d_p$. (c) $\tilde{w} > d_p$; $\tilde{w} > d_u - d_p$. (d) $\tilde{w} < d_p$; $\tilde{w} > d_u - d_p$.

TABLE II

ANALYSIS OF MOTION BLUR EFFECTS ON A PERIODIC PULSE SIGNAL

Case	MIG	$var\left[p'(x)\right]$
$\tilde{w} = 1$ (No motion blur)	$\frac{2a}{d_u}$	$\frac{2a^2}{d_u}$
$\tilde{w} < d_p$; $\tilde{w} < d_u - d_p$	$\frac{2a}{d_u}$	$\frac{2a^2}{d_u \cdot \tilde{w}}$
$\tilde{w} > d_p$; $\tilde{w} < d_u - d_p$	$\frac{2a \cdot d_p}{\tilde{w} \cdot d_u}$	$\frac{2a^2 \cdot d_p}{\tilde{w}^2 \cdot d_u}$
$\tilde{w} > d_p$; $\tilde{w} > d_u - d_p$	$\frac{2a}{\tilde{w}} \cdot \left(1 - \frac{\tilde{w}}{d_u}\right)$	$\frac{2a^2}{\tilde{w}^2} \cdot \left(1 - \frac{\tilde{w}}{d_u}\right)$
$\tilde{w} < d_p$; $\tilde{w} > d_u - d_p$	$\frac{2a}{\tilde{w}} \cdot \left(1 - \frac{d_p}{d_u}\right)$	$\frac{2a^2}{\tilde{w}^2} \cdot \left(1 - \frac{d_p}{d_u}\right)$

The analysis of the results of calculation clearly highlights that motion blur is able to decrease the values of both MIG and $SSSIG$. Those parameters, as shown in the literature, drive the description of uncertainty, in particular decreasing $SSSIG$ increase uncertainty u_e. Nonetheless, the analysis of this simple model returns the following findings.

1) The $SSSIG$ is linearly dependent on the variance of image gradient, rather than being dependent on the value of MIG. This finding is also useful since the variance of image gradient can be calculated easily with spectral methods, given the premises of (10).

2) The behavior of image degradation with motion blur is not continuous. In fact, the analysis of convolution states the existence of four cases of interest, as detailed in the next points.

3) At low $\tilde{w}$ level, motion blur affects the strength of edges, but not contrast [Fig. 4(a)]. As shown in Table II, in this situation MIG is not altered by motion blur, while the $SSSIG$ decreases. Consequently, this is an edge loss driven phenomenon (i.e., edge strength decreases as $\tilde{w}$ increases).

4) As motion blur increases [Fig. 4(b) and (c)], image contrast is lowered, $SSSIG$ decreases with higher pace with respect to edge driven phenomenon, and uncertainty is driven by contrast loss.

5) When patterns are particularly rich [as in the case of Fig. 4(d)], the in-center spacing of pulses d_u is low and it is possible to have a simultaneous loss of edges and contrast even at low levels of motion blur.

Now that the effects of motion blur in the corruption of signal are described, it is possible to evaluate what are the consequences on correlation.

A. Correlation of Original Signal With a Motion Blurred One

Since the formulation of motion blurred signal is available, it is now possible to analyze what happens when correlating
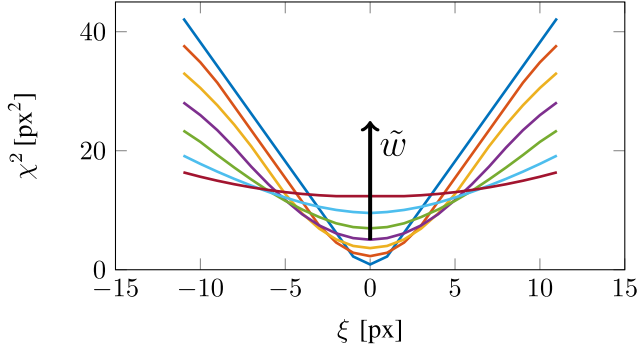
Fig. 5. Minimum of cross-correlation function as $\tilde{w}$ increases. Computation with $a = 1$, $d_u = 20$, $d_p = 10$, and $1 \leq \tilde{w} \leq 21$.
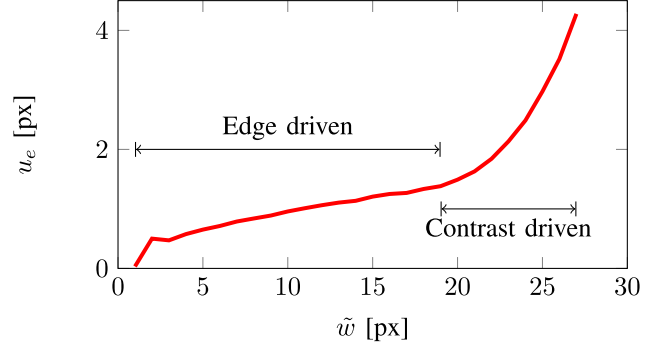

Fig. 6. Displacement uncertainty when correlating the original signal with a blurred one. Motion blur is tested at a really high level for didactic purposes.

the reference signal $p_o(x)$ with a blurred one $p_b(x)$, so that the correlation problem can be addressed analytically. This case is similar to DIC vibration monitoring, where the reference image is usually shot when target lies motionless in the equilibrium position while the correlating image is affected by motion blur. This condition is a worst case scenario, since, as demonstrated in [5], the magnitude of random errors decreases when the blur level of the two images is similar. This model relies on continuous signals even if images are sampled at a pixel level; therefore, in the model, the interpolation that is usually done on images to allow subpixel correlation is not implemented. Although simpler than the actual image correlation problem, continuous signal approaches are still helpful to qualitatively understand the behavior of uncertainty, as demonstrated in [51]. With reference to the methodology of Sutton *et al.* [51], it is possible to calculate the correlation function $\chi^2(\xi)$ in (12), which represents the sum of squared differences (SSD). The variable ξ is the exact pixel shift of $p_b(x)$ with respect to $p_o(x)$

$$\chi^2(\xi, \tilde{w}) = [p_b(x - \xi, \tilde{w}) - p_o(x)]^2. \quad (12)$$

Considering only the case of Fig. 4(a), it is possible to calculate the value of the correlation function for a subset of N periods and then linearize the behavior around small values of $\tilde{w}$ and ξ in (13). As motion blur $\tilde{w}$ increases, the minimum of $\chi^2(\xi, \tilde{w})$ becomes higher and flatter, as shown in Fig. 5, where the results of (13) are displayed

$$\chi^2(\xi, \tilde{w}) \approx Na^2 \cdot \left(\frac{\tilde{w}}{4} + \frac{2}{\tilde{w}} \xi^2 \right). \quad (13)$$

However, when noise is added to signals, the correlation match is variable and, consequently, uncertainty starts to arise when recovering displacement. To go further in the derivation, it is necessary to add a Gaussian noise $\tau_i(x)$ having variance equal to σ^2 to each image. Following the derivation proposed by Sutton *et al.* [51], this is equal to adding a noise-dependent term $\tau(\xi)$ to the correlation function

$$\tau(\xi) = N\sigma^2 (1 + P + Q \cdot \xi). \quad (14)$$

The coefficient P and Q linearize the correlation score induced by noise in each image around the exact match position. In particular, P represents the *SSD* of noise and Q noise

correlation score. Hence, the correlation function becomes

$$\chi^2(\xi) \approx Na^2 \cdot \left(\frac{\tilde{w}}{4} + \frac{2}{\tilde{w}} \xi^2 \right) + N\sigma^2 (1 + P + Q \cdot \xi). \quad (15)$$

Consequently, it is possible to calculate the correlation drift due to noise and motion blur ξ_M, as the minimum point of correlation function [so that $(d/d\xi)\chi^2 = 0$ gives (16)]

$$\xi_M = \frac{\sigma^2 Q \cdot \tilde{w}}{4a^2}. \quad (16)$$

Equation (16) demonstrates that the correlation drift is directly proportional to the power of noise as well as to the amount of motion blur. This is a major finding, since it demonstrates that motion blur $\tilde{w}$ plays a role similar to an increment of noise as an uncertainty driving factor.

B. Evaluation With a Monte Carlo Simulation

The previous analysis is limited to one of the motion blurring cases highlighted in Table II (i.e., $\tilde{w} < d_p$; $\tilde{w} < d_u - d_p$, which is a condition often verified by practical applications). In order to validate the whole theoretical construction, a Monte Carlo simulation is run ($a = 1$, $d_p = 6$, $d_u = 22$, $\sigma = 0.05$, $1 \leq \tilde{w} \leq 27$). In this case, several levels of motion blur are tested, and then, for each of them, noise signals τ_o and τ_b are sampled and added to signals $p_o(x)$ and $p_b(x)$. Consequently, correlation is run and displacement is calculated as the minimum point of $\chi^2(\xi)$. The imposed relative displacement between the original signal and the correlating one is identically equal to 0. For each level of motion blur $\tilde{w}$, correlation is tested 10^4 times. Hence, uncertainty $u_e(\tilde{w})$ is evaluated as the standard deviation of measured displacement at each level of motion blur. The result is displayed in Fig. 6.

It is interesting to compare the results displayed in Fig. 6 with the previous analysis. Equation (16) computes the correlation drift for a given realization of noise pattern and for a given value of $\tilde{w}$. In addition, (16) predicts a linear growth of uncertainty with motion blur and this is reflected by the diagram in Fig. 6. Furthermore, the previous analysis predicted the existence of an edge driven region [analyzed by (16)] and a contrast-driven region. The transition between the two regions is predicted when $\tilde{w} = d_u - d_p$, then u_e should grow faster. This behavior is also reflected by the data in Fig. 6 and it is
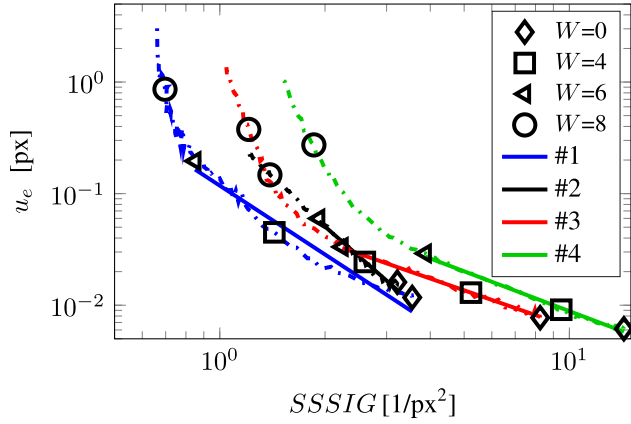
Fig. 7. Linear logarithmic dependence $SSSIG - u_e$. Dashed line: data. Solid line: model.

Fig. 8. Solid line: contrast loss. Dashed line: model error.

Fig. 9. Dependence $SSSIG - W$. Dashed line: data. Solid line: model.

a natural consequence of having the $SSSIG$ decreasing with quadratic pace at high levels of motion blur.

VI. POWER-LAW MODEL TO DESCRIBE UNCERTAINTY AS A FUNCTION OF MOTION BLUR WIDTH

The analysis of the monodimensional model cannot be directly extended to the case of a general image of a DIC measurement pattern. However, findings and remarks of the previous analysis are useful to understand the driving factors of uncertainty arising with motion blur. Consequently, it is possible to formulate interpretative model upon physical basis. In this context, the hypothesis made is to relax the constraint given by (2) in order to include in the analysis the effect of motion blur and to express the relationship between uncertainty u_e due to random error (evaluated as the standard deviation of subset displacement) and $SSSIG$ with a simple power law as in (17)

$$u_e = \frac{\eta}{(SSSIG)^\alpha}. \tag{17}$$

The previous equation represents a linear function in the logarithmic plane where parameter η represents the sensitivity of uncertainty to both noise and motion blur [since the two phenomena mix, as demonstrated by (16)]. Parameter α, instead, represents the speed of degradation of correlation accuracy as the motion blur increases. It is possible to retrieve the coefficients from regression of experimental data. The process is shown in Fig. 7.

In Fig. 7 it is possible to see that not all the field of motion blur is covered by the model. In fact, as shown in the previous section, the interaction between image correlation, noise, and motion blur splits the behavior of uncertainty in two parts: an edge driven interval and a contrast driven interval. The power law model, in fact, aims to represent the linear degradation due to edge loss, which is the one at the lower level of W, which is very interesting in most of the practical applications. The previous assumptions are verified in Fig. 8, where both the modulus of model error (computed as the discrepancy between the actual value of the uncertainty and the uncertainty value predicted by the model) and the contrast ratio (the ratio between the contrast of the static image and the contrast of the
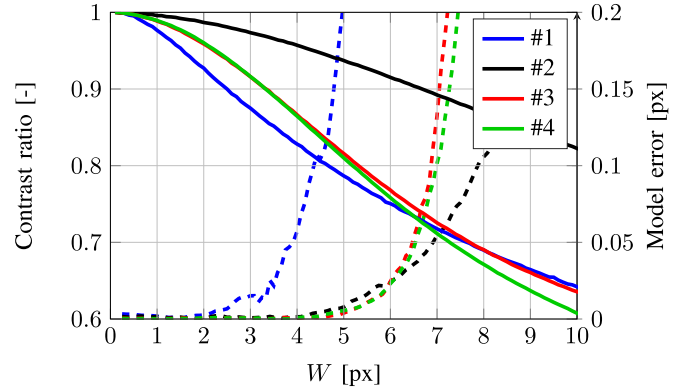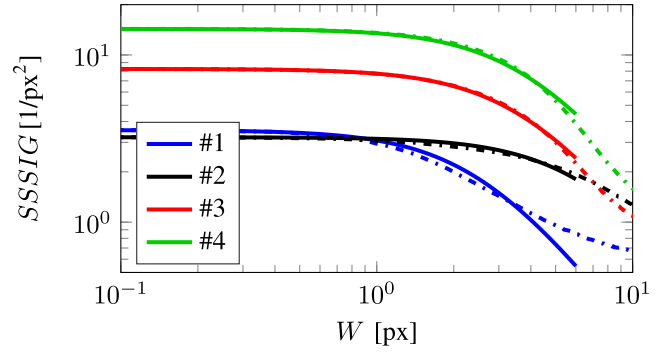
motion blurred one) are plotted. It is possible to see that the fit error increases as contrast decreases. Contrast decreases with different pace depending on the pattern peculiar shape so that similar patterns behave similarly. Pattern with a good resistance in terms of contrast loss (for instance, patterns characterized by a larger d_u/d_p ratio) are more resistant to motion blur (in terms of measurement uncertainty).

The next step is to model the interaction between $SSSIG$ and motion blur W. The monodimensional analysis proposes a quadratic dependence; hence, it is possible to write (18), where $SSSIG_0$ represents the value of $SSSIG$ in static conditions and β represents the pattern degradation factor, which represents the sensitivity to motion blur

$$SSSIG(W) = \frac{SSSIG_0}{\beta \cdot W^2 + 1}. \tag{18}$$

As shown in Fig. 9, the model correctly interpolates the data with R^2 scores higher than 92% for patterns #2, #3, and #4. For what concerns pattern #1, the discrepancy is slightly larger for $W > 4$. This is likely due to the very low contrast of the pattern, coupled with a very small size of the speckle. Given all the previous analysis, eq.19 updates the uncertainty model expressed with eq.17. In this way it is possible to include the effects of motion blur in the analysis of uncertainty.

$$u_e(W) = \frac{\eta}{[SSSIG(W)]^\alpha} = \frac{\eta}{\left(\frac{SSSIG_0}{\beta \cdot W^2 + 1}\right)^\alpha}. \tag{19}$$

As shown in Fig. 10, the model is able to correctly predict the behavior of uncertainty, given the amount of motion blur.
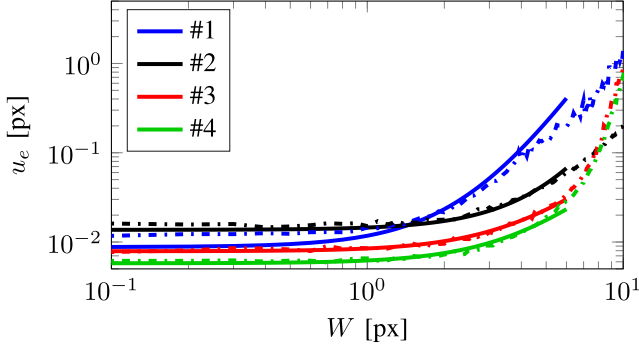
Fig. 10. Power law model is able to express the relationship between uncertainty and motion blur. Dashed: data. Solid: model.
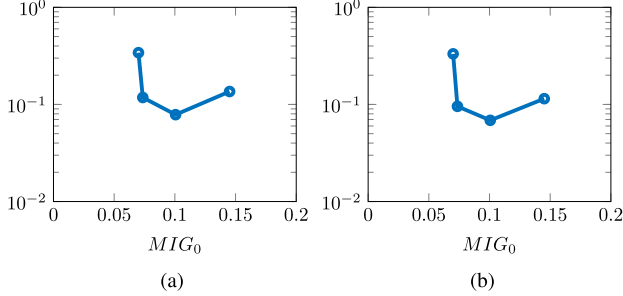

(a)   (b)

Fig. 11. Sensitivity of model parameters to the static value of MIG for the acquired pattern. (a) η parameter. (b) MBRF parameter.

It is also possible to approximate the value of $SSSIG_0$ with the Pan formula, given that it refers to static conditions; hence, it is possible to write

$$u_e(W) \approx \frac{\eta}{\left(\frac{N^2 \cdot MIG_0^2}{\beta \cdot W^2 + 1}\right)^\alpha} \approx \frac{\eta \cdot (\beta \cdot W^2 + 1)^\alpha}{(N \cdot MIG_0)^{2\alpha}}. \tag{20}$$

The model of (19) has been validated with four different patterns, as shown in Fig. 1. Linearizing (20) leads to the following expression:

$$u_e(W) \approx u_e(0) + \left.\frac{d\,u_e}{d\,W}\right|_0 \cdot W + \left.\frac{d^2\,u_e}{d\,W^2}\right|_0 \cdot W^2. \tag{21}$$

Then the following approximation for the behavior of uncertainty with motion blur is retrieved:

$$u_e(W) \approx \frac{\eta}{(N \cdot MIG_0)^{2\alpha}} \cdot (1 + 2\alpha\beta W^2). \tag{22}$$

This last expression is particularly interesting, since it demonstrates that an optimization of pattern under dynamic conditions is possible and useful. The uncertainty due to motion blur is regulated by the rational constant of (22), which is defined as the motion blur rejection factor (MBRF). Both the numerator and denominator vary with MIG. In this case, an analytic definition of $\eta(MIG_0)$ is not available; however, given that, in general, numerator and denominator vary differently with MIG_0, it is possible to suppose the existence of an optimal point.

In fact, by representing the model parameters η and $MBRF$ as a function of MIG_0 in Fig. 11, it is possible to see that uncertainty is not linearly decreasing with the mean image gradient. In particular, both the indexes describe how the quality of correlation is affected by both noise and motion blur. Increasing the MIG_0 of patterns on one hand improves

the rejection of the effects of noise, but, on the other hand, the accumulation of edges in a small space facilitates the loss of contrast in motion blur conditions.

In other words, it is not possible to boost static performances and dynamic performances at the same time. This explains why accurate DIC measurement is a more complex task and, in the end, it is necessary to develop tools in order to select optimal patterns for a given application.

VII. CONCLUSION

This paper approached the problem of modeling 2-D DIC displacement measurement uncertainty in dynamic conditions. Motion blur conditions have been generated synthetically using a set of well-known algorithms. The review of the scientific literature provided us with uncertainty models developed for static applications. As a consequence, we analyzed the effects of motion blur on correlation process starting from the case of monodimensional signals. In this way, it was possible to mathematically derive the sensitivity of SSD correlation function to the amount of motion blur. Once the monodimensional case has been fully recovered, the extension to a general image case has been carried out by means of a power-law match score that is able to take into account both the noise and the motion blur. In this way, it was possible to reproduce the results of simulation and to provide a suitable framework to predict uncertainty in the context of 2-D DIC measurements tasks.

REFERENCES

[1] M. Bornert *et al.*, "Assessment of digital image correlation measurement errors: Methodology and results," *Experim. Mech.*, vol. 49, no. 3, pp. 353–370, 2009.

[2] B. Pan, "Bias error reduction of digital image correlation using Gaussian pre-filtering," *Opt. Lasers Eng.*, vol. 51, no. 10, pp. 1161–1167, 2013.

[3] H. W. Schreier, J. R. Braasch, and M. A. Sutton, "Systematic errors in digital image correlation caused by intensity interpolation," *Opt. Eng.*, vol. 39, no. 11, pp. 2915–2921, 2000.

[4] Y. Wang, P. Lava, S. Coppieters, M. De Strycker, P. van Houtte, and D. Debruyne, "Investigation of the uncertainty of dic under heterogeneous strain states with numerical tests," *Strain*, vol. 48, no. 6, pp. 453–462, 2012.

[5] E. Zappa, A. Matinmanesh, and P. Mazzoleni, "Evaluation and improvement of digital image correlation uncertainty in dynamic conditions," *Opt. Lasers Eng.*, vol. 59, pp. 82–92, Aug. 2014.

[6] E. Hack, X. Lin, E. A. Patterson, and C. M. Sebastian, "A reference material for establishing uncertainties in full-field displacement measurements," *Meas. Sci. Technol.*, vol. 26, no. 7, p. 075004, 2015.

[7] D. Wang, Y. Jiang, W. Wang, and Y. Wang, "Bias reduction in subpixel image registration based on the anti-symmetric feature," *Meas. Sci. Technol.*, vol. 27, no. 3, p. 035206, 2016.

[8] P. Mazzoleni, F. Matta, E. Zappa, M. A. Sutton, and A. Cigada, "Gaussian pre-filtering for uncertainty minimization in digital image correlation using numerically-designed speckle patterns," *Opt. Lasers Eng.*, vol. 66, pp. 19–33, Mar. 2015.

[9] M. W. Nansteel and C. C. T. Chen, "Digital image correlation: A measurement tool for the study of explosive effects," in *Proc. IEEE Conf. Technol. Homeland Secur. (HST)*, May 2009, pp. 234–241.

[10] X. Li, W. Xu, M. A. Sutton, and M. Mello, "*In situ* nanoscale in-plane deformation studies of ultrathin polymeric films during tensile deformation using atomic force microscopy and digital image correlation techniques," *IEEE Trans. Nanotechnol.*, vol. 6, no. 1, pp. 4–12, Jan. 2007.

[11] O. V. Lychak and I. S. Holyns'kiy, "Evaluation of random errors in Williams' series coefficients obtained with digital image correlation," *Meas. Sci. Technol.*, vol. 27, no. 3, p. 035203, 2016.

[12] F. A. Sadjadi, "Performance evaluations of correlations of digital images using different separability measures," *IEEE Trans. Pattern Anal. Mach. Intell.*, vol. 4, no. 4, pp. 436–441, Jul. 1982.

[13] P. L. Reu, W. Sweatt, T. Miller, and D. Fleming, "Camera system resolution and its influence on digital image correlation," *Experim. Mech.*, vol. 55, no. 1, pp. 9–25, 2015.

[14] P. Lava, W. Van Paepegem, S. Coppieters, I. De Baere, Y. Wang, and D. Debruyne, "Impact of lens distortions on strain measurements obtained with 2D digital image correlation," *Opt. Lasers Eng.*, vol. 51, no. 5, pp. 576–584, 2013.

[15] L. Yu and B. Pan, "The errors in digital image correlation due to overmatched shape functions," *Meas. Sci. Technol.*, vol. 26, no. 4, p. 045202, 2015.

[16] G. Crammond, S. W. Boyd, and J. M. Dulieu-Barton, "Speckle pattern quality assessment for digital image correlation," *Opt. Lasers Eng.*, vol. 51, no. 12, pp. 1368–1378, 2013.

[17] G. Lionello and L. Cristofolini, "A practical approach to optimizing the preparation of speckle patterns for digital-image correlation," *Meas. Sci. Technol.*, vol. 25, no. 10, p. 107001, 2014.

[18] S. Ma, J. Pang, and Q. Ma, "The systematic error in digital image correlation induced by self-heating of a digital camera," *Meas. Sci. Technol.*, vol. 23, no. 2, p. 025403, 2012.

[19] S. Wang, X. Yao, Q. Su, and Y. J. Ma, "High temperature image correction in DIC measurement due to thermal radiation," *Meas. Sci. Technol.*, vol. 26, no. 9, p. 095006, 2015.

[20] M. A. Iadicola, "Uncertainties of digital image correlation due to pattern degradation at large strain," in *Proc. Annu. Conf. Experim. Appl. Mech.*, vol. 3. 2016, pp. 247–253.

[21] Y. Wang, P. Lava, P. Reu, and D. Debruyne, "Theoretical analysis on the measurement errors of local 2D DIC: Part II assessment of strain errors of the local smoothing method–approaching an answer to the overlap question," *Strain*, vol. 52, no. 2, pp. 129–147, 2016.

[22] C. Cofaru, W. Philips, and W. van Paepegem, "Evaluation of digital image correlation techniques using realistic ground truth speckle images," *Meas. Sci. Technol.*, vol. 21, no. 5, p. 055102, 2010.

[23] P. L. Reu, "A realistic error budget for two dimension digital image correlation," in *Proc. Annu. Conf. Experim. Appl. Mech.*, vol. 3. 2016, pp. 189–193.

[24] T. Schmidt, J. Tyson, and K. Galanulis, "Full-field dynamic displacement and strain measurement using advanced 3D image correlation photogrammetry: Part I," *Experim. Techn.*, vol. 27, no. 3, pp. 47–50, 2003.

[25] T. Schmidt, J. Tyson, and K. Galanulis, "Full-field dynamic displacement and strain measurement—Specific examples using advanced 3D image correlation photogrammetry: Part II," *Experim. Techn.*, vol. 27, no. 3, pp. 22–26, 2003.

[26] J. Sicard and J. Sirohi, "Measurement of the deformation of an extremely flexible rotor blade using digital image correlation," *Meas. Sci. Technol.*, vol. 24, no. 6, p. 065203, 2013.

[27] K. Chang, A. Nazare, and P. Ifju, "Flapping wing deformation measurement in hover flight conditions," in *Proc. Annu. Conf. Experim. Appl. Mech.*, vol. 3. 2016, pp. 143–149.

[28] J. Baqersad, P. Poozesh, C. Niezrecki, and P. Avitabile, "Photogrammetry and optical methods in structural dynamics—A review," *Mech. Syst. Signal Process.*, vol. 86, pp. 17–34, Mar. 2016.

[29] M. N. Helfrick, C. Niezrecki, P. Avitabile, and T. Schmidt, "3D digital image correlation methods for full-field vibration measurement," *Mech. Syst. Signal Process.*, vol. 25, no. 3, pp. 917–927, 2011.

[30] C. Warren, C. Niezrecki, P. Avitabile, and P. Pingle, "Comparison of FRF measurements and mode shapes determined using optically image based, laser, and accelerometer measurements," *Mech. Syst. Signal Process.*, vol. 25, no. 6, pp. 2191–2202, 2011.

[31] W. Wang, J. E. Mottershead, A. Ihle, T. Siebert, and H. R. Schubach, "Finite element model updating from full-field vibration measurement using digital image correlation," *J. Sound Vibrat.*, vol. 330, no. 8, pp. 1599–1620, 2011.

[32] P. Poozesh, J. Baqersad, C. Niezrecki, P. Avitabile, E. Harvey, and R. Yarala, "Large-area photogrammetry based testing of wind turbine blades," *Mech. Syst. Signal Process.*, vol. 86, pp. 98–115, Mar. 2016.

[33] P. Poozesh, J. Baqersad, C. Niezrecki, and P. Avitabile, "A multi-camera stereo DIC system for extracting operating mode shapes of large scale structures," in *Proc. Annu. Conf. Experim. Appl. Mech.*, vol. 3. 2016, pp. 225–238.

[34] D. A. Ehrhardt, M. S. Allen, S. Yang, and T. J. Beberniss, "Full-field linear and nonlinear measurements using continuous-scan laser Doppler vibrometry and high speed three-dimensional digital image correlation," *Mech. Syst. Signal Process.*, vol. 86, pp. 82–97, Mar. 2016.

[35] E. Zappa, P. Mazzoleni, and A. Matinmanesh, "Uncertainty assessment of digital image correlation method in dynamic applications," *Opt. Lasers Eng.*, vol. 56, pp. 140–151, May 2014.

[36] G. Busca, G. Ghislanzoni, and E. Zappa, "Indexes for performance evaluation of cameras applied to dynamic measurements," *Measurement*, vol. 51, pp. 182–196, May 2014.

[37] Z. Wang, H. Kieu, H. Nguyen, and M. Le, "Digital image correlation in experimental mechanics and image registration in computer vision: Similarities, differences and complements," *Opt. Lasers Eng.*, vol. 65, pp. 18–27, Feb. 2015.

[38] Y. Wang, P. Lava, P. Reu, and D. Debruyne, "Theoretical analysis on the measurement errors of local 2D DIC: Part I temporal and spatial uncertainty quantification of displacement measurements," *Strain*, vol. 52, no. 2, pp. 110–128, 2015.

[39] A. Lavatelli and E. Zappa, "Modeling uncertainty for a vision system applied to vibration measurements," *IEEE Trans. Instrum. Meas.*, vol. 65, no. 8, pp. 1818–1826, Aug. 2016.

[40] Society Experimental Mechanics. *DIC Challenge*, accessed on Feb. 1, 2016. [Online]. Available: http://sem.org/dic-challenge

[41] P. L. Reu, "Experimental and numerical methods for exact subpixel shifting," *Experim. Mech.*, vol. 51, no. 4, pp. 443–452, 2011.

[42] G. Busca, A. Cigada, P. Mazzoleni, and E. Zappa, "Vibration monitoring of multiple bridge points by means of a unique vision-based measuring system," *Experim. Mech.*, vol. 54, no. 2, pp. 255–271, 2014.

[43] Y. Q. Wang, M. A. Sutton, H. A. Bruck, and H. W. Schreier, "Quantitative error assessment in pattern matching: Effects of intensity pattern noise, interpolation, strain and image contrast on motion measurements," *Strain*, vol. 45, no. 2, pp. 160–178, 2009.

[44] Z. Gao, X. Xu, Y. Su, and Q. Zhang, "Experimental analysis of image noise and interpolation bias in digital image correlation," *Opt. Lasers Eng.*, vol. 81, pp. 46–53, Jun. 2016.

[45] Y. Su, Q. Zhang, Z. Gao, X. Xu, and X. Wu, "Fourier-based interpolation bias prediction in digital image correlation," *Opt. Exp.*, vol. 23, no. 15, pp. 19242–19260, 2015.

[46] B. Pan, Z. Lu, and H. Xie, "Mean intensity gradient: An effective global parameter for quality assessment of the speckle patterns used in digital image correlation," *Opt. Lasers Eng.*, vol. 48, no. 4, pp. 469–477, 2010.

[47] P. Reu, "All about speckles: Speckle size measurement," *Experim. Techn.*, vol. 38, no. 6, pp. 1–2, 2014.

[48] P. Reu, "All about speckles: Contrast," *Experim. Techn.*, vol. 39, no. 1, pp. 1–2, 2015.

[49] P. Reu, "All about speckles: Edge sharpness," *Experim. Techn.*, vol. 39, no. 2, pp. 1–2, 2015.

[50] P. Reu, "All about speckles: Speckle density," *Experim. Techn.*, vol. 39, no. 3, pp. 1–2, 2015.

[51] M. Sutton, J. Orteu, and H. Schreier, *Image Correlation for Shape, Motion and Deformation Measurements: Basic Concepts, Theory and Applications*. New York, NY, USA: Springer, 2009.

Alberto Lavatelli (M'14) received the M.Sc. degree in mechanical engineering from the Polytechnic University of Milan, Milan, Italy, in 2015, where he is currently pursuing the Ph.D. degree with the Department of Mechanical Engineering.

His current research interests include the development of vision-based techniques applied to mechanical and thermal measurements.

Emanuele Zappa (M'10) received the Ph.D. degree in applied mechanics from the Polytechnic University of Milan, Milan, Italy, in 2002.

In 2001, he joined the Department of Mechanical Engineering, as a Researcher, where he is currently an Associate Professor at the Dept. of Mechanical Engineering at the Polytechnic University of Milan, Milan, Italy.

He has authored several publications in the field of measurements, with a focus on vision-based techniques: digital image correlation, 3-D structured light scanning, and stereoscopy.

Dr. Zappa's original contribution covers the development, the improvement, and the uncertainty analysis of the aforementioned techniques, as well as their application in complex and harsh environments.